

Towards the prediction of soot in aero-engine combustors with large eddy simulation

By B. Cuenot[†], E. Riber[†] AND B. Franzelli

A simplified methodology is proposed to calculate soot production in aeronautical burners. It is based on reduced chemistry, used to propagate the flame, coupled to tabulated chemistry to describe the soot precursors. These precursors are then introduced in a two-equation soot model accounting for the major source and sink terms of soot concentration. To validate this approach, the computation is also performed with a fully tabulated chemistry approach and the same soot model. Results are compared in the configuration of Geigle *et al.* (2014) for which OH, temperature, and soot measurements are available.

1. Motivation and objectives

Soot forming is the result of a complex heterogeneous chemical process, where gaseous precursors trigger the formation of solid particles that may aggregate and react on their surface. Like combustion, this chemical phenomenon is also very sensitive to turbulent transport and mixing, which makes soot highly intermittent and strongly dependent on the temporal and spatial evolution of the flow.

Many experimental studies have dealt with turbulent diffusion flames in academic configurations, focusing on soot chemistry in a well-defined and simple flow (Lee *et al.* 2009; Köhler *et al.* 2012). Only a few studies (Lammel *et al.* 2007; Meyer *et al.* 2005) consider complex turbulent flows in realistic geometries as it is very difficult to obtain the necessary information from experiment in such configurations. Nevertheless, Geigle *et al.* (2014) have recently published both flame and soot measurements in a turbulent swirl-stabilized ethylene-air flame, providing valuable inputs to soot model validation.

At the same time, numerical simulation, either Reynolds Averaged Navier Stokes (RANS) or Large Eddy Simulation (LES), has become an essential tool to improve and design combustion systems, providing complementary and unique information compared to experiment at substantially lower cost. RANS simulations of sooting flames (Pitsch *et al.* 2000; Blacha *et al.* 2011) have proven to be effective for a good description of mean flow quantities, but they fail to describe the local and unsteady mechanisms of soot production (Köhler *et al.* 2012). By solving the most energetic large scales of the flow, LES succeeds in capturing intermittent turbulent flow structures and is therefore very promising for soot modeling. LES has already led to significant advances in the description of unsteady combustion phenomena at a reasonable computational cost. It has recently been applied to soot production in turbulent flames, confirming the feasibility of the approach, but was mostly limited to laboratory-scale configurations (El-Asrag *et al.* 2007; Donde *et al.* 2013). Mueller & Pitsch (2013) were the first to compute soot production in a real aeronautical burner, including a detailed description of gaseous chemistry (with a tabulated chemistry approach) and the soot particle motion and chemistry (using

[†] CERFACS, France

a method of moments). Lecocq *et al.* (2014) also studied a real helicopter chamber with a reduced gaseous chemistry and a phenomenological soot model, reducing the cost of the simulations. In these studies, numerous modeling and numerical issues have not yet been completely solved, and validation of the models by comparison with measurements in real complex flows typical of aero-engines is still lacking.

This work proposes to evaluate the LES approach to predict soot production in the swirl-stabilized non-premixed ethylene/air aero-engine combustor studied at DLR by Geigle *et al.* (2014), for which flame and soot data are available. A simple, still reasonable, two-equation soot model (Leung *et al.* 1991) is used, combined with the hybrid chemical description proposed by Lecocq *et al.* (2014) (reduced chemistry for the flame structure/tabulated chemistry for soot precursors) or to a full-tabulated chemistry method (Vicquelin *et al.* 2011). First, these two chemistry descriptions along with the two-equation soot model are compared in a rich laminar premixed ethylene-air flame. Then, they are applied to the DLR ethylene-air aero-engine combustor computed with LES. Temperature field and soot concentration obtained in the two LES are validated against experimental results, and the sensitivity to the chemical models is investigated.

2. Methodology for soot modeling

2.1. Gaseous reacting flow modeling

Soot particles appear after a nucleation process, resulting from the collisions of Polycyclic Aromatic Hydrocarbons (PAHs) in the gas phase. The formation of PAHs involves the creation of first aromatic rings (such as benzene) from which heavier compounds are formed via the HACA cycles. As PAHs collisions increase with temperature, due to an increase of the Brownian motion of particles, the fuel oxidation mechanism must be accurately described. After nucleation, soot mass increases and/or decreases according to particle growth, condensation, and oxidation at the particle surface. These mechanisms are highly dependent on the concentration of some gaseous intermediate species such as acetylene, OH, and O₂. Accounting for all these phenomena is CPU-consuming, and three main simplifications have been adopted in this study. First, fuel oxidation is described either by a classical fully tabulated method (Vicquelin *et al.* 2011) or by a hybrid technique (reduced chemistry for the flame structure/tabulated chemistry for soot precursor chemistry) proposed by Lecocq *et al.* (2014). Second, acetylene is considered as the sole soot precursor (Leung *et al.* 1991; Lecocq *et al.* 2014). Finally, the retroaction of the soot particles on the flame (thermal radiation, species consumption) is neglected (Zhu & Gore 2005). Among the numerous detailed mechanisms available for ethylene-air combustion, the one developed by Wang & Laskin (1998) (75 species and 529 reactions, referred to as WL) has been retained as a reference because it correctly reproduces not only the flame speed, the temperature, and the flame structure but also the gaseous intermediate species such as acetylene and OH.

2.1.1. Fully tabulated method

Tabulation methods allow a decrease in the computational cost of the chemical description by assuming that the chemical evolutions can be described by a reduced manifold. These methods have recently been used to perform LES of sooting flames (Donde *et al.* 2013). The FPI-TTC (Vicquelin *et al.* 2011) approach used in this work considers that ethylene-air chemistry can be described by the mixture fraction Y_z^{fpi} , based on carbon atom conservation and assuming unity Lewis number for all species, and

the normalized progress variable $c^{fpi} = Y_c^{fpi}/Y_c^{eq}$, where $Y_c^{fpi} = Y_{CO} + Y_{CO_2}$ is the classical progress variable. These two variables Y_z^{fpi} and c^{fpi} read classical transport equations (Vicquelin *et al.* 2011), and the flame structure is recovered from a look-up table, built from unstrained premixed laminar flames solutions. Here, 310 premixed laminar flames ($0.026 < Y_z^{fpi} < 0.192$, i.e., $0.4 < \phi < 3.50$) have been computed using the detailed WL mechanism in CANTERA to create the look-up table with 1000×100 points for the mixture fraction and the progress variable, respectively. The operating conditions, fresh gas temperature $T_f = 300$ K and pressure $P = 3$ atm, are those of the target application (Geigle *et al.* 2014).

2.1.2. Hybrid method

Reduced chemistries are commonly used to decrease the computational cost by reducing the number of species and reactions while preserving the accuracy of quantities of interest. However, these reduced schemes do not contain the gaseous precursors that trigger soot production (El-Asrag *et al.* 2007). To overcome this problem, Lecocq *et al.* (2014) proposed a hybrid technique coupling a two-step reduced chemistry for fuel oxidation with a tabulation method to describe precursor species. In this work, acetylene is the only soot precursor, but the approach could be easily extended to heavier and more complex precursors.

The fuel oxidation is described by a two-step six-species reduced scheme for laminar premixed ethylene-air flames, referred to as 2S-C2H4-BFER hereafter, and built with the methodology proposed by Franzelli *et al.* (2012). The first reaction controls the flame speed and the second reaction represents the CO – CO2 equilibrium. Reaction rates are modeled by Arrhenius laws corrected with a pre-exponential adjustment function of the equivalence ratio $f_j(\phi)$ in order to correctly reproduce the flame speed of rich mixtures (Franzelli *et al.* 2012). The Arrhenius law parameters are the same as those for the methane-air two-step scheme in Franzelli *et al.* (2012), except that the fuel oxidation pre-exponential factor $A_1 = 2.10^{10}$ and the CO – CO2 equilibrium temperature exponent $\beta_2 = 0.8$. Unity Lewis numbers are assumed for all species, together with a constant Prandtl number $Pr = 0.7$. Following Lecocq *et al.* (2014), acetylene is recovered from the same look-up table built for the fully tabulated method. To couple the reduced chemistry to the look-up table, a mixture fraction $Y_z^{red} = Y_z^{fpi}$ and a progress variable c^{red} are defined and calculated from the reduced scheme variables. Since the burnt gas composition is different between reduced and detailed descriptions, c^{red} cannot be directly evaluated as Y_c^{fpi} . Lecocq *et al.* (2014) define the normalized progress variable c^{red} as

$$c^{red}(Y_z^{red}) = \begin{cases} 1 - Y_{C_2H_4}/Y_z^{red} & \text{if } \phi \leq 1.0, \\ 1 - Y_{O_2}/0.233/(1 - Y_z^{red}) & \text{if } \phi \geq 1.0. \end{cases} \quad (2.1)$$

This definition is, however, not adequate to describe the radical recombination and the post-flame region, and an additional progress variable c^{tr} is introduced as the solution to the following transport equation

$$\frac{\partial c^{tr}}{\partial t} + \frac{\partial}{\partial x_i} (\rho u_i c^{tr}) = \frac{\partial}{\partial x_i} \left(\rho D \frac{\partial c^{tr}}{\partial x_i} \right) + \dot{\omega}_c^{tr}, \quad (2.2)$$

This equation is associated to boundary conditions of 0 in the fresh gas and 1 in the burnt gas. The reaction rate $\dot{\omega}_c^{tr}$ is built to match c^{red} in the flame zone and c^{fpi} in the

Step	A_i	n_i	T_i	Unity
Nucleation	$2.80 \cdot 10^8$	0	21100	$[\text{s}^{-1}]$
Surface growth	$1.4 \cdot 10^2$	0	12100	$[\text{m}^3 \text{m}_{soot}^{-2} \text{s}^{-1}]$
O ₂ oxidation	$1.4 \cdot 10^5$	0.5	19680	$[\text{m}^3 \text{m}_{soot}^{-2} \text{s}^{-1}]$
OH oxidation	$1.484 \cdot 10^3$	-0.5	0	$[\text{kmol} \text{m}_{soot}^{-2} \text{s}^{-1}]$

TABLE 1. Reaction parameters for the two-equation soot model. The functions of temperature $k_i(T)$ of Eqs. (2.4)-(2.5) are given by: $k_i(T) = A_i T^{n_i} e^{-T_i/T}$.

post-flame region, with a transition at the value c^* (here $c^* = 0.5$)

$$\dot{\omega}_c^{tr}(c^{tr}, Y_z^{red}) = \begin{cases} \dot{\omega}_c^{red} = (c^{red} - c^{tr})/\tau^* & \text{if } c^{tr} < c^* , \\ \dot{\omega}_c^{tab}(c^{tr}, Y_z^{red}) & \text{if } c^{tr} > c^* , \end{cases} \quad (2.3)$$

where $\tau^* = 5.0\Delta t$ guarantees a smooth relaxation from c^{tr} to c^{red} (Lecocq *et al.* 2014).

2.2. Soot modeling

The two-equation soot model derived from Leung *et al.* (1991) is evaluated here with the two gas chemistry methods. The soot mass fraction Y_s , and the number density of soot particles n_s , are solutions to the following equations

$$\begin{aligned} \frac{\partial \rho n_s}{\partial t} + \frac{\partial}{\partial x_i} (\rho v_i n_s) &= k_T \frac{\partial}{\partial x_i} \left(\frac{\rho \nu n_s}{T} \frac{\partial T}{\partial x_i} \right) + \frac{2}{C_{min}} N_A k_1(T^{tab}) [\text{C}_2\text{H}_2]^{tab} \\ &\quad - 2C_a \left(\frac{6M_s}{\pi \rho_s} \right)^{1/6} \left(\frac{6\kappa T^{tab}}{\rho_s} \right)^{1/2} (\rho^{tab} n)^{11/6} \left(\frac{\rho^{tab} Y_s}{M_s} \right)^{1/6}, \quad (2.4) \\ \frac{\partial \rho Y_s}{\partial t} + \frac{\partial}{\partial x_i} (\rho v_i Y_s) &= k_T \frac{\partial}{\partial x_i} \left(\frac{\rho \nu Y_s}{T} \frac{\partial T}{\partial x_i} \right) \\ &\quad + k_1(T^{tab}) [\text{C}_2\text{H}_2]^{tab} M_s + k_2(T^{tab}) [\text{C}_2\text{H}_2]^{tab} f(S) M_s \\ &\quad - (k_3(T^{tab}) [\text{O}_2]^{tab} + \varphi_{OH} k_4(T^{tab}) X_{OH}^{tab}) S M_s, \quad (2.5) \end{aligned}$$

where $[X]$ is the concentration of species X in kmol.m^{-3} , M_s and ρ_s are the soot molar mass and density, N_A and κ are Avogadro and Boltzmann constants. The quantities extracted from the look-up table with both the fully tabulated and the hybrid methods are indicated by the superscript *tab*. As the temperature and the density obtained with the reduced mechanism and the look-up table can differ greatly in the post-flame for rich mixtures, the density and the temperature extracted from the look-up table are used to evaluate the soot source terms when using the hybrid method. The same constants as in Lecocq *et al.* (2014) have been used: $k_T = 0.54$, $C_a = 9.0$, $C_{min} = 100.0$, $\kappa = 1.38 \cdot 10^{-23}$, $\rho_s = 2000 \text{ kg.m}^{-3}$, and $M_s = 12.011 \text{ kg.kmol}^{-1}$. Only the oxidation by OH has been reduced by multiplying the source term by $\varphi_{OH} = 0.3$, and the reaction rate constants A_i , n_i , and T_i have been adapted to reproduce correct soot profiles in laminar premixed ethylene-air flames (Section 3) and are provided in Table 1.

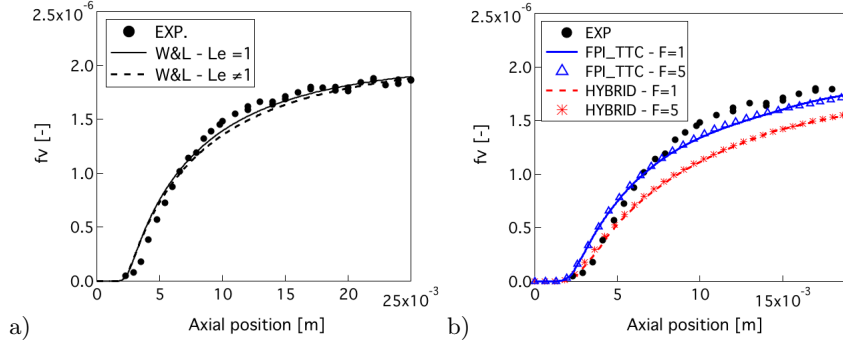


FIGURE 1. Soot volume fraction profile for the laminar premixed flame at $T_f = 300\text{ K}$, $P = 3\text{ atm}$, and $\phi = 2.30$. Comparison between experimental (symbols) and numerical results (lines). Effect of a) unity Lewis number assumption using the WL detailed mechanism, and b) gas chemistry model and artificially thickened flame model.

2.3. Coupling with turbulence

The artificially thickened flame model (Colin *et al.* 2000; Charlette *et al.* 2002) is used to account for the sub-grid interaction between turbulence and chemistry. To be consistent, thickening is also applied to the equations for Y_c^{tr} , n_s , and Y_s . The same sensor based on $\dot{\omega}_{Y_c^{tr}}$ is used for both the fully tabulated and the hybrid methods.

3. Validation in 1D laminar premixed ethylene-air flames

The performances of the two models - fully tabulated chemistry or hybrid method - coupled to the two-equation soot model are first evaluated in a one-dimensional laminar premixed ethylene-air flame at the operating conditions of the target configuration (Geigle *et al.* 2014). The experimental results of Tsurikov *et al.* (2005), providing both temperature and soot volume fraction f_v profiles at equivalence ratio $\phi = 2.3$ for the same conditions, are used for validation. The flame has first been calculated using the detailed WL mechanism with CANTERA, the soot volume fraction being *a posteriori* calculated by integrating the two equations of the soot model with the set of constants summarized in Section 2.2 (Figure 1(a)). The effect of unity Lewis number on soot concentration is also shown in Figure 1(a), using the WL mechanism and unity Lewis number for all species. As expected, the impact of the unity Lewis number on the soot volume fraction is small, allowing the use of look-up tables and reduced chemistry built with this assumption. This reference solution is then compared to the results obtained with the compressible solver AVBP (Gourdain *et al.* 2009), using the simplified gas chemical descriptions (Figure 1(b)). Small discrepancies between the fully tabulated and hybrid methods are observed due to the different definitions of the progress variable, but the overall agreement is satisfactory.

Finally the impact of the combustion model has been evaluated by thickening the flame front with a constant factor $\mathcal{F} = 5$. Results are also shown in Figure 1(b), where for the sake of clarity, the axial coordinate has been divided by \mathcal{F} for the two thickened flames. The agreement with the non-thickened results is good, proving that the thickening process does not change the soot production in laminar flames.

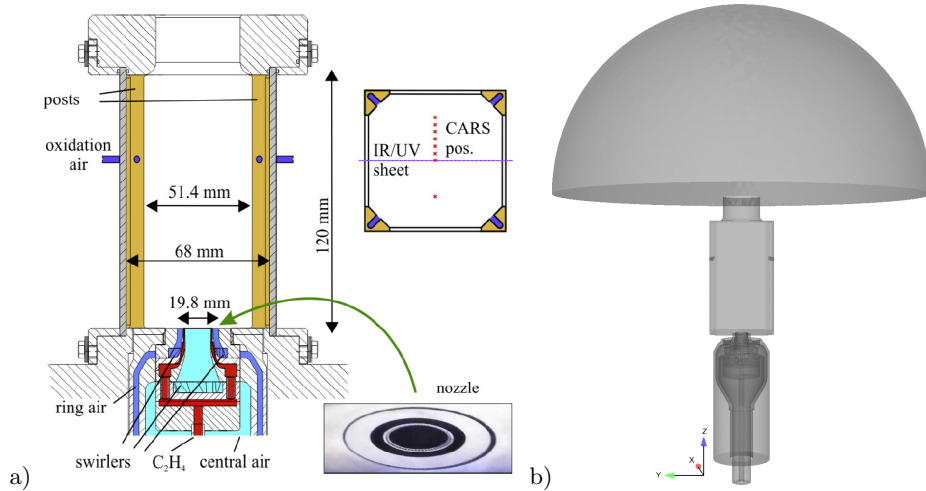


FIGURE 2. a) Experimental configuration from Geigle *et al.* (2014). b) Computational domain

4. LES of a turbulent swirl-stabilized ethylene-air flame experiment

4.1. Description of the experimental setup

The injection device in the burner experienced by Geigle *et al.* (2014) is composed of three concentric nozzles and two radial swirlers (Figure 2(a)). Air is fed through both a central nozzle followed by a radial swirler consisting of 8 channels (the swirl number is $Sw=0.82$) and an annular nozzle followed by a radial swirler composed of 11 channels ($Sw=0.78$). Gaseous ethylene is injected in between both air flows through 60 straight channels forming a concentric ring (Figure 2(a)). The combustion chamber is 120 mm long, has a square section of $68 \times 68 \text{ mm}^2$, and is equipped with quartz windows allowing optical access. Secondary air can be injected through additional ducts located on the combustion chamber at a height of 80 mm. The combustor operates at about 10kW/bar thermal power providing Reynolds numbers larger than 10,000. Coherent anti-Stokes Raman scattering was used for temperature measurements, laser-induced incandescence for soot concentration, and laser-induced fluorescence for the determination of OH radical distributions. The operating point studied in this work is $P = 3 \text{ bars}$, $Q_{air,central} = 140.8 \text{ l.mn}^{-1}$, $Q_{air,radial} = 328.5 \text{ l.mn}^{-1}$, $Q_{fuel} = 39.3 \text{ l.mn}^{-1}$, leading to an injection equivalence ratio of $\phi = 1.2$. As air is injected through additional ducts $Q_{oxi} = 187.4 \text{ l.mn}^{-1}$, the global equivalence ratio is $\phi_{global} = 0.86$.

4.2. Numerical setup

The computational domain is displayed in Figure 2(b). It includes the whole injection system, the combustion chamber and the secondary air ducts, and extends downstream of the combustion chamber to take into account a part of the outside atmosphere, where a non-reflecting outlet boundary condition at 3 bar is imposed. The domain is discretized into a fully unstructured mesh using approximately 17 million tetrahedra. The axial direction is referred to as the z -axis. All simulations are performed with AVBP, an explicit cell-vertex massively parallel code solving compressible reacting flows. The second-order accurate in space and time Lax-Wendroff numerical scheme is used. Inlet and outlet boundary conditions are treated according to the Navier-Stokes Characteristic Boundary Conditions formulation, and walls are considered adiabatic non-slipping. Turbulent

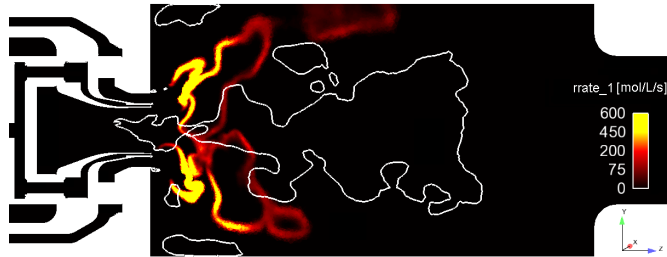


FIGURE 3. Instantaneous fuel oxidation reaction rate field with zero axial velocity isoline in the mid-plane $x = 0$ mm using the hybrid method.

subgrid stresses are modeled using the WALE approach, while the subgrid diffusive heat and species fluxes are modeled with constant turbulent Prandtl and Schmidt numbers, respectively ($Pr_t = Sc_{t,k} = 0.6$). Two LES have been performed, using either the fully tabulated chemistry or the hybrid method coupled to the two-equation soot model.

4.3. Results

4.3.1. Flow and flame structure

The turbulent flow structure is first illustrated using the results of the hybrid method (Figure 3). The swirled injection leads to a central recirculation zone that extends downstream to $z \simeq 90$ mm and penetrates inside the injector device by 10 mm. This recirculation zone is accompanied by a corner recirculation zone located all around the burner at the bottom, where the temperature stays relatively low (Figure 4(a)). This flow structure is classical for swirled flows and consistent with a swirl number of about 0.8. The trace of the oxidation jets at $z = 80$ mm is also visible on both the velocity and temperature fields.

Figure 4(a) compares the mean temperature field obtained with both the fully tabulated and the hybrid method. The flame is similar in both cases, naturally stabilizing in the recirculation zone very close to the tip of the recirculation zone. It takes the classical conical shape obtained in such a swirled flow and it extends downstream to $z \simeq 8$ mm without impacting the chamber walls. The flame is mostly premixed, burning at equivalence ratios ranging from 0.86 to 1.2. Comparison with experiment is made in Figure 5 where the mean temperature axial profile is shown for both chemical descriptions. The agreement is satisfactory for both approaches, with a correct profile shape but an overestimated temperature in the burnt gas. A shorter flame core is observed when using the hybrid method, as discussed in Franzelli *et al.* (2013). The fuel oxidation is almost complete at $z \approx 0.025$ m, where the maximum temperature value (2400K) is found (the burnt gas temperature corresponding to the combustor global equivalence ratio is 2290K). Downstream, due to air injection through the additional tubes, the gas temperature is cooled down, and the burnt gas composition changes near the chamber exit.

4.3.2. Soot production

Figure 4(b) shows the mean field of acetylene mass fraction obtained by the hybrid approach and the fully tabulated approach. As in 1D flames, acetylene appears in the hot gas region and reaches levels about $5 \cdot 10^{-3}$, i.e., sufficient to trigger soot production. The levels and distribution of acetylene concentration are quite similar between the two approaches, which confirms the correct behavior of the hybrid reduced/tabulated chemistry approach in a complex turbulent flow. This is an important finding of the present work

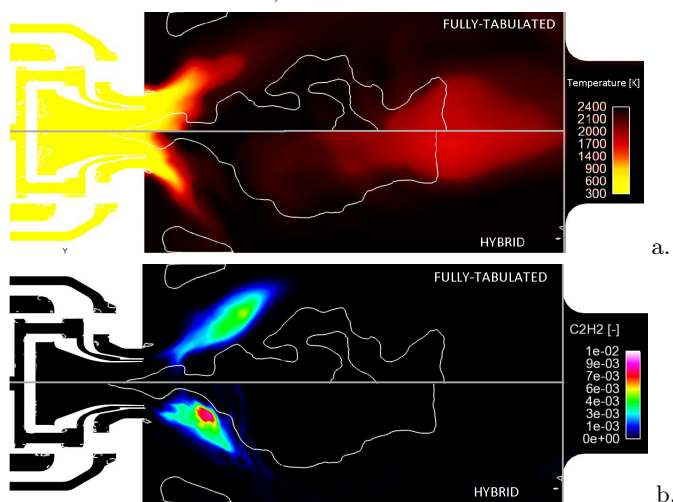


FIGURE 4. Time-averaged fields of a) temperature and b) acetylene (C_2H_2) in the mid-plane $x = 0$ mm. Comparison between fully tabulated (top) and hybrid (bottom) methods.

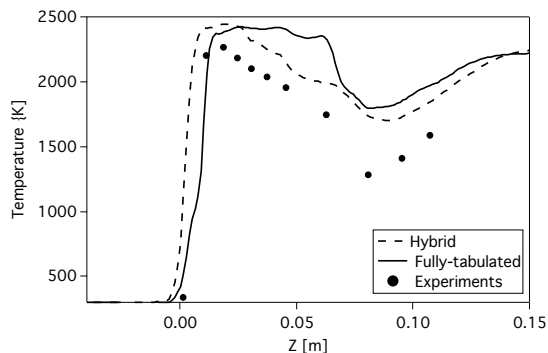


FIGURE 5. Axial profile of mean temperature. Comparison between experiment from Geigle *et al.* (2014) (symbols), fully tabulated (solid line) and hybrid (dashed line) methods. The chamber inlet corresponds to $z = 0$ mm.

as it shows that detailed chemical information required to compute pollutants can be reconstructed from a reduced kinetic in agreement with the classical tabulation method.

The instantaneous distributions of OH and soot are qualitatively compared to experimental results in Figure 6. In agreement with the experimental data, the OH concentration is localized in the whole chamber due to the injection downstream of additional air and, in particular, into the inner recirculation zone. Soot ligaments are then confined by the OH concentration due to the soot-OH oxidation and are not likely to be found in the inner recirculation zone. This feature is correctly reproduced by both simulations, although a very simple soot model was used. This result is encouraging and demonstrates the capacity of LES to capture the main global features of soot production.

5. Conclusions and perspectives

A hybrid method coupling reduced chemistry for fuel oxidation and tabulated chemistry for soot precursors has been evaluated against a fully tabulated approach and ex-

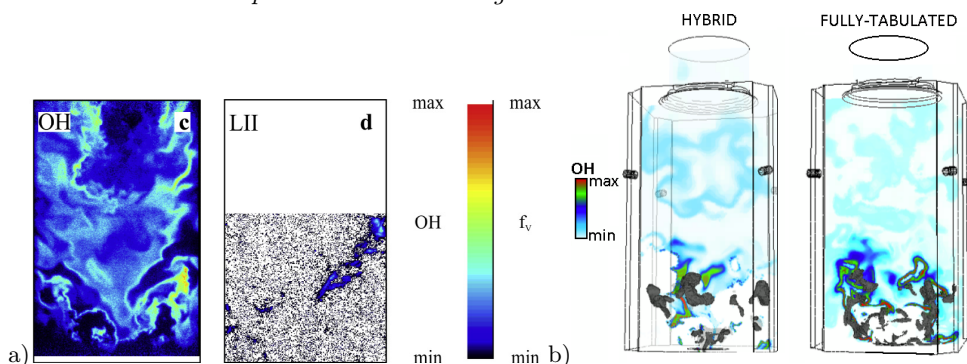


FIGURE 6. Instantaneous fields of a) OH and b) soot. Comparison between experiment from Geigle *et al.* (2014) (left), hybrid (middle), and fully tabulated (right) methods where soots are represented by a gray volume fraction isosurface.

periment in both a laminar premixed flame and a lab-scale aeronautical burner. Results confirm that the hybrid approach is suitable for soot modeling, combining the advantages of maintaining explicit Arrhenius laws for the chemistry of combustion along with those of tabulated chemistry for pollutants. The results of the comparison with measured soot concentration in a complex configuration are encouraging, especially considering the very simple soot model that has been used. The hybrid approach can now be extended to more accurate - albeit still reduced - chemical descriptions and coupled to more sophisticated soot models to improve the prediction capability of simulation for soot production.

REFERENCES

- BLACHA, T., DOMENICO, M. D., GERLINGER, P. & AIGNER, M. 2011 Modeling of soot and NOX in a full scale turbine engine combustor with detailed chemistry. In *Proceedings of the ASME Turbo Expo*, pp. GT2011-45084.
- CHARLETTE, F., MENEVEAU, C. & VEYNANTE, D. 2002 A power-law flame wrinkling model for LES of premixed turbulent combustion. Part I: non-dynamic formulation and initial tests. *Combust. Flame* **131**, 159–180.
- COLIN, O., DUCROS, F., VEYNANTE, D. & POINSOT, T. 2000 A thickened flame model for Large Eddy Simulations of turbulent premixed combustion. *Phys. Fluids* **12**, 1843–1863.
- DONDE, P., RAMAN, V., MUELLER, M. E. & PITSCH, H. 2013 LES/PDF based modeling of soot-turbulence interactions in turbulent flames. *Proc. Combust. Inst.* **34**, 1183 – 1192.
- EL-ASRAG, H., LU, T., LAW, C. & MENON, S. 2007 Simulation of soot formation in turbulent premixed flames. *Combust. Flame* **150**, 108–126.
- FRANZELLI, B., RIBER, E. & CUENOT, B. 2013 Impact of the chemical description on a Large Eddy Simulation of a lean partially-premixed swirled flame. *C. R. Mécanique* **341**, 247–256.
- FRANZELLI, B., RIBER, E., GICQUEL, L. Y. M. & POINSOT, T. J. 2012 Large Eddy Simulation of combustion instabilities in a lean partially premixed swirled flame. *Combust. Flame* **159**, 621–637.
- GEIGLE, K., KÖHLER, M., O’LOUGHLIN, W. & MEIER, W. 2014 Investigation of soot

- formation in pressurized swirl flames by laser measurements of temperature, flame structures and soot concentrations. *Proc. Comb. Inst.*, In Press.
- GOURDAIN, N., GICQUEL, L., MONTAGNAC, M., VERMOREL, O., GAZAIX, M., STAFFELBACH, G., GARCÍA, M., BOUSSUGE, J.-F. & POINSOT, T. 2009 High performance parallel computing of flows in complex geometries - part 1: methods. *Comput Sci Discov.* **2**, 015003.
- KÖHLER, M., GEIGLE, K.-P., BLACHA, T., GERLINGER, P. & MEIER, W. 2012 Experimental characterization and numerical simulation of a sooting lifted turbulent jet diffusion flame. *Combust. Flame* **159**, 2620–2635.
- LAMMEL, O., GEIGLE, K., LÜCKERATH, R., MEIER, W. & AIGNER, M. 2007 Investigation of soot formation and oxidation in a high-pressure gas turbine model combustor by laser techniques. In *Proceedings of GT2007, ASME Turbo Expo 2007: Power of Land, Sea and Air, May 14-17, 2007, Montreal, Canada*, pp. GT2007–27902.
- LECOCQ, G., POITOU, D., HERNANDEZ, I., DUCHAINE, F., RIBER, E. & CUENOT, B. 2014 LES model for sooting turbulent nonpremixed flames. *Flow, Turb. and Combustion* **92**, 947–970.
- LEE, S.-Y., TURNS, S. & SANTORO, R. 2009 Measurements of soot, OH, and PAH concentrations in turbulent ethylene/air jet flames. *Combust. Flame* **156**, 2264–2275.
- LEUNG, K., LINDSTEDT, R. & JONES, W. 1991 A simplified reaction mechanism for soot formation in nonpremixed flames. *Combust. Flame* **87**, 289 – 305.
- MEYER, T., ROY, S., BELOVICH, V., CORPORAN, E. & GORD, J. 2005 Simultaneous planar laser-induced incandescence, OH planar laser-induced fluorescence, and droplet Mie scattering in swirl-stabilized spray flames. *Appl. Opt.* **44**, 445–454.
- MUELLER, M. & PITSCH, H. 2013 Large Eddy Simulation of soot evolution in an aircraft combustor. *Physics of Fluids* **25**, 110812.
- PITSCH, H., RIESMEIER, E. & PETERS, N. 2000 Unsteady flamelet modeling of soot formation in turbulent diffusion flames. *Combust. Sci. Technol.* **158**, 389 – 406.
- TSURIKOV, M., GEIGLE, K., KRUGER, V., SCHNEIDER-KUHNLE, Y., STRICKER, W., LUCKERATH, R., HADEF, R. & AIGNER, M. 2005 Laser-based investigation of soot formation in laminar premixed flames at atmospheric and elevated pressures. *Combust. Sci. Technol.* **177** (10), 1835–1862.
- VICQUELIN, R., FIORINA, B., PAYET, S., DARABIHA, N. & GICQUEL, O. 2011 Coupling tabulated chemistry with compressible CFD solvers. *Proc. Comb. Inst.* **33**, 1481–1488.
- WANG, H. & LASKIN, A. 1998 *A comprehensive kinetic model of ethylene and acetylene oxidation at high temperatures*. Internal report, Department of Mechanical and Aerospace Engineering, Princeton University.
- ZHU, X. & GORE, J. 2005 Radiation effects on combustion and pollutant emissions of high-pressure opposed flow methane/air diffusion flames. *Combust. Flame* **141**, 118 – 130.